ELBERT AND SAINT-SÉVERIN: LL6 (S4) CHONDRITES WITH CONTRASTING SHOCK HISTORIES.

R.C. Hugo[1], A.M. Ruzicka[1], and A.E. Rubin[2]. [1]Portland State University, Portland, OR; hugo@pdx.edu, [2]University of California – Los Angeles.

INTRODUCTION

We utilized optical microscopy (OM), transmission electron microscopy (TEM), and electron backscatter diffraction (EBSD) methods with a focus on the mineral olivine, to study the shock histories of two LL6 chondrites – Elbert and Saint-Séverin. Using OM we assigned a weighted shock stage to each specimen according to the method of Jamsja and Ruzicka [1]. We mapped thin sections using EBSD to determine deformation intensity via misorientation maps, crystallographic texture via pole figures, and mesoscale slip plane analysis via crystal rotation figures. Areas of interest were prepared via Focused Ion Beam lift-out technique for TEM analysis of dislocation character and density. Although both meteorites are classified [2] as shock-stage S4, our results show that they have significantly different shock histories.

Elbert **is a relatively uniform, fine-grained specimen with a weighted shock stage of S4.4 ± 0.9 (n=35 grains), featuring many olivine grains with S4 characteristics and a considerable proportion (28%) with S5 or S6 characteristics. EBSD slip plane analysis shows that c-type slip predominates, with evidence for slip on multiple slip planes or unconstrained cross-slip. TEM evidence reveals a dislocation structure of c-type dislocations with long, straight screw segments and relatively short, straight edge segments. This is consistent with slip constrained to {hk0} planes, indicating relatively cool shock temperatures. Dislocation densities range from 1×10^{13}–5×10^{14} m^{-2}, consistent with an S4 or higher shock stage. We found very few low angle grain boundaries.**

Elbert EBSD

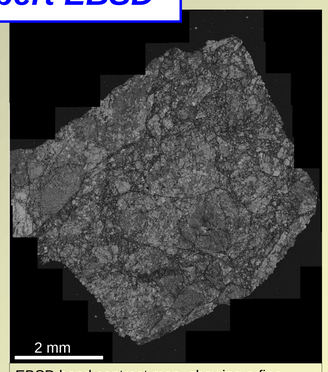

EBSD band contrast map, showing a fine microstructure laced with fractures. Most of this structure is of relatively low porosity.

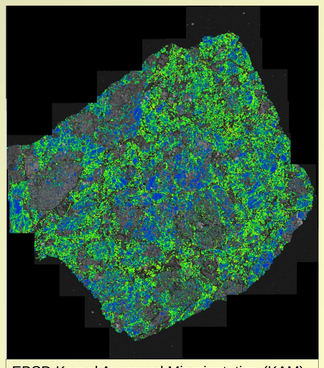

EBSD Kernel Averaged Misorientation (KAM) map. Blue-to-red heat map indicates each pixel's misorientation with respect to neighboring pixels. Only olivine grains are shown. This map shows a highly deformed but relatively uniform structure.

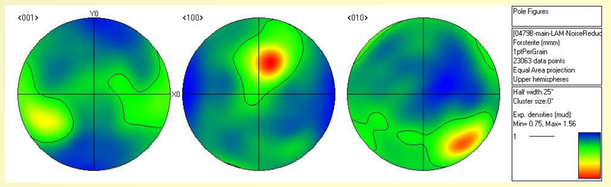

Above - EBSD olivine pole figures with a maximum density of 1.56 (in units of MUD - multiple of uniform density) indicate a very weak lattice preferred orientation.

At right - Crystal Rotation Axis (CRA) figure shows a preferred rotation axis of <010>, consistent with deformation dominated by slip on the [001](010) system. Significant densities along the <100> - <010> trace indicate some cross slip has occurred, e.g. [001](hk0) slip. CRA figures for the isolated clasts do not differ significantly from the whole-section figure at right.

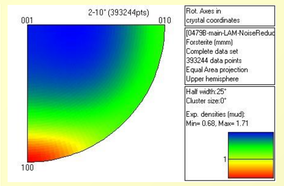

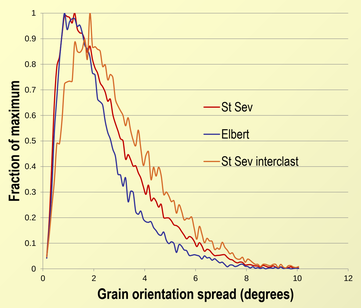

Grain Orientation Spread (GOS) distributions for both Elbert and St Severin. A relatively extended distribution indicates a general lack of dislocation recovery or recrystallization. Note higher spread angles, both of the distribution peak and the distribution tail, for the St Severin interclast subset.

Saint-Séverin **has a brecciated texture, with low-porosity clasts separated by higher porosity interclast regions. Olivine grains in clasts range from S2 to S4, with a corresponding weighted shock stage of S3.2 ± 1.2 (n=247). EBSD misorientation maps show that plastic strain is heterogeneously distributed both among and within clasts, in agreement with OM data indicating a large dispersion of deformation. However, EBSD slip-plane analysis suggests that the six distinct clasts in our specimen experienced similar slip system temperatures. TEM evidence reveals a predominance of curved and looped c-type dislocations within the clasts, with no evidence of thermal recovery or annealing, suggesting that the clasts were deformed at a moderately elevated temperature. Dislocation densities in these clasts range from 1×10^{10} – 5×10^{13} m^{-2}, consistent with S2-S4 shock values. In highly deformed regions between clasts, however, we found fine-grained olivine with a high proportion of a-type dislocations. These a-type dislocations are arranged in sub-planar arrays forming subgrain boundaries, whereas c-type dislocations are randomly distributed. Dislocation densities in these regions are 1×10^{13} – 1×10^{14} m^{-2}, which would be consistent with S4 shock values.**

St Severin EBSD

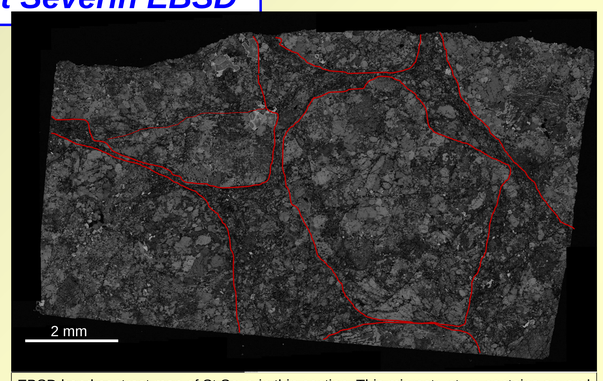

EBSD band contrast map of St Severin thin section. This microstructure contains several distinct low-porosity clasts separated by a high porosity interclast region. Clasts are outlined in red.

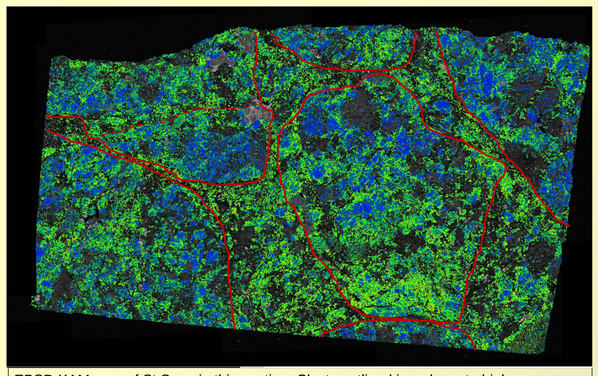

EBSD KAM map of St Severin thin section. Clasts outlined in red – note higher misorientations in and near the interclast region.

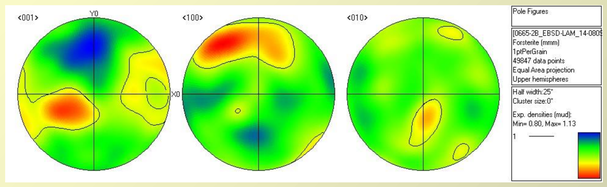

Above - EBSD olivine pole figures with a maximum density of 1.13 MUD indicate no significant lattice preferred orientation.

At right - CRA figure shows a preferred rotation axis of [010], consistent with deformation dominated by slip on either [001](100) or [100](001). Significant densities along the <100> - <010> trace indicate some cross slip on [001](hk0) has occurred and suggests the dominant system is [001](100). CRA figures for the isolated clasts do not differ significantly from the whole-section figure at right.

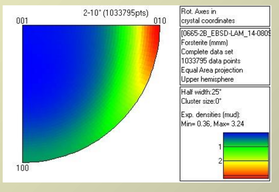

Elbert TEM

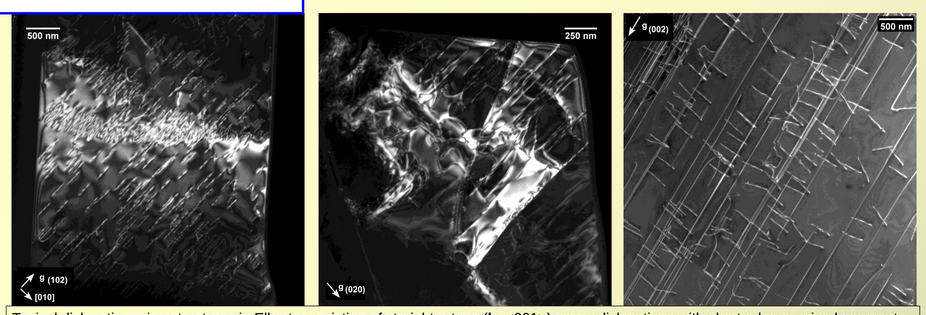

Typical dislocation microstructures in Elbert, consisting of straight **c**-type (**b**=<001>) screw dislocations with short edge or mixed segments. **a**-type (**b**=<100>) dislocations are rare (<~5%). Dislocation density ranges from 1×10^{13}–5×10^{14} m^{-2} , and low angle grain boundaries are rare.

St Severin clast TEM

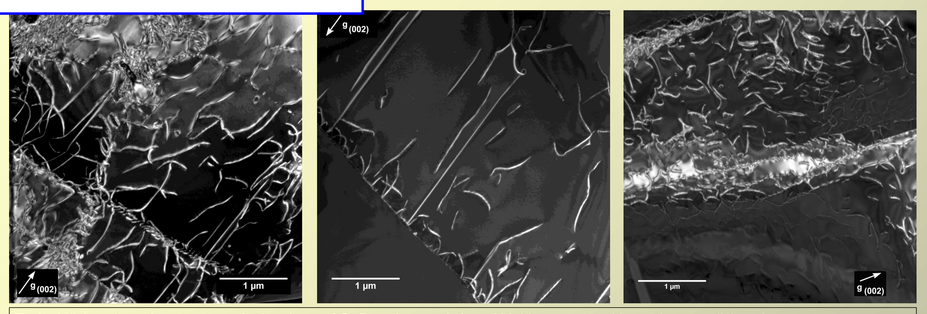

Typical dislocation microstructures in the clasts of St Severin, consisting of highly curved and looped **c**-type dislocations. **a**-type dislocations are rare, <~5%. Dislocation densities range from 1×10^{10} – 5×10^{13} m^{-2} .

St Severin interclast TEM

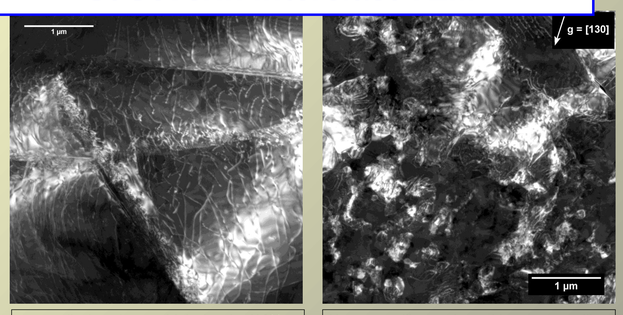

c-type disclocations at high density (10^{14} m^{-2}). Note presence of dislocations "bound" in planar arrays. These low angle boundaries are more common in the interclast.

Nanocrystalline region, with nanocrystalline domains delineated by sub-planar arrays of **a**-type dislocations. **c**-type dislocations, which are not visible in this image, are rare in this region.

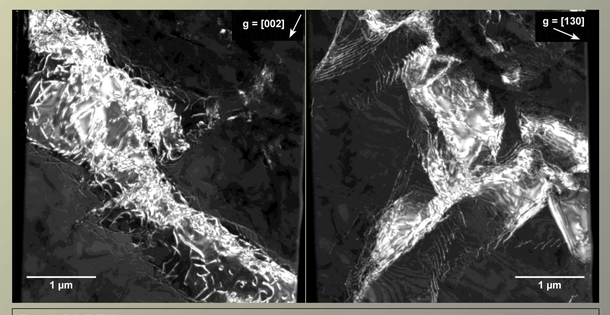

Two WBDF TEM images of the same area under different diffraction conditions. Left, **c**-type dislocations visible; right, **a**-type visible. Note that **c**-type dislocations are "free" while **a**-type dislocations are "bound" in sub-planar arrays, indicating more rapid recovery of **a**-types.

Conclusions: **Although both meteorites are shock-stage S4 and neither shows evidence for significant post-shock annealing, they otherwise experienced significantly different shock histories. Elbert experienced a strong shock from a cold initial to a cold ending state with no significant shock-induced heating. Shock deformation may have involved some crushing of grains to result in a predominantly small grain size. In contrast, Saint-Séverin shows evidence for elevated temperature during shock and rapid post-shock cooling. The clastic structure of Saint-Séverin implies a complex history in which low-porosity clasts were lithified prior to a final shock event that produced the dislocation microstructures we observed. Within the clasts, c-type slip with extensive cross-slip and/or dislocation climb suggests that temperature was moderately elevated but insufficient to activate high-temperature slip systems. In interclast areas, the high proportion of a-type dislocations suggests higher temperature deformation, while high dislocation densities suggest high temperatures were caused by localized shock heating in what were likely shear zones. Cooling was slow enough to allow some recovery of a-type dislocations but rapid enough to prevent significant recovery of c-type dislocations. This complex history may have led to the seemingly contradictory histories previously inferred [3,4].**

References: [1] Jamsja N. and Ruzicka A. (2010) *Meteoritics & Planetary Science* 45, 828-849. [2] Stöffler D. et al. (1991) *Geochimica et Cosmochimica Acta* 55, 3845-3867. [3] Ashworth J.R. (1981) *Proceedings of the Royal Society London A* 374, 179-194. [4] Leroux H. et al. (1996) *Meteoritics & Planetary Science* 31, 767-776.

Acknowledgments: This work was supported by NASA, grant NNX14AF39G. All electron microscopy was performed at PSU's Center for Electron Microscopy and Nanofabrication

Abstract 6298, 80th annual meeting of the Meteoritical Society (2017).